AIAA AVIATION Forum
5-9 June 2017, Denver, Colorado
47th AIAA Fluid Dynamics Conference

10.2514/6.2017-3817

On the passive pitching mechanism in turning flapping flights using a torsional spring model

Qiang Zhong[1], Geng Liu[2], Yan Ren[3], and Haibo Dong[4]
Department of Mechanical and Aerospace Engineering
University of Virginia, Charlottesville, VA 22904

Abstract

In this work, we propose a three-dimensional passive pitching model of a flapping wing in pure yaw turn maneuver. The flapping and deviation motions are prescribed, but the interaction among the torsional spring, aerodynamic torques, and inertia torques governs the pitching motion. The aerodynamic forces and the unsteady flow are simulated by an in-house immersed-boundary-method based computational fluid dynamics (CFD) solver. The ratio of yaw angle rotation velocity to flapping velocity range from 0 to 0.25 are simulated with *Re=300* and stroke amplitude $\phi = 120^{\circ}$. The simulation results indicate the yaw angle rotation has significant impacts on both the aerodynamic performance and vortex structure. Specially, the yaw angle rotation strengths the leading-edge vortex (LEV) of the wing and maintains a longer period for high angle of attack during the half-stroke in which flapping direction is same as yaw turn direction. It is also found the yaw angle rotation makes kinematic and aerodynamic asymmetric and increases the lift generation by 10.4% at yaw angle rotation velocity to flapping velocity ratio is 0.25. The findings of this work indicate the passive pitching mechanism may have great impacts on flapping flyer maneuver.

Keywords: *insect flight, torsional spring, passive pitching, maneuver, lift, asymmetric pitching, computational fluid dynamics*

Nomenclature

A	Wing area
c	Mid-chord length
AR	Aspect ratio
C_D	Instantaneous drag coefficient and cycle-averaged drag coefficient, respectively
C_L	Instantaneous lift coefficient and cycle-averaged lift coefficient, respectively
C_P	Pressure coefficient
ω_f	Flapping velocity
f	Flapping frequency
f_n	Natural frequency
K	Elastic modulus of torsional spring
M_{aero}	Aerodynamic torque
$M_{elastic}$	Elastic generated
$M_{gravity}$	Torque generated by gravitational force
Re	Reynolds number
θ	Pitch angle
ϕ	Stroke angle
α	Deviation angle
α_m	Deviation amplitude
Ω	Yaw angle rotation velocity

[1] Ph.D. Student, AIAA student member, qz4te@virginia.edu
[2] Research Associate, AIAA member, gl6d@virginia.edu
[3] Research Associate, AIAA member, yr5my@virginia.edu
[4] Associate Professor, AIAA Associate Fellow, haibo.dong@virginia.edu

I. Introduction

Flapping-wing propulsion is the most common motion type in flying animals and insects. There has been substantial interest in such motion over past decades due to its high maneuverability and efficiency compared to fixed-wing flight and rotorcraft. Understanding the flapping kinematics control mechanism is necessary for the design of micro air vehicle (MAV). In files, there exists a high torsional flexibility area in the narrow basal and short root region[1,2], which can result in the passive pitching motion during flapping.

Tremendous research and studies have been done in passive pitching mechanism. The passive pitching motion is governed by the combination of elastic force of wing, the aerodynamics force and the moment inertia of the wing[3,4]. Ishihara et al.[3] investigated the passive pitching due to wing torsional flexibility and lift generation in dipteran flight, and demonstrated that enough lift could be produced to support the weight of some dipterans. Bergou et al.[5] calculated rotational power about the torsion axis is owing to aerodynamic and wing inertial forces and suggested that the aerodynamic and inertial forces are sufficient to pitch the wing without the aid of the muscles. Whitney et al.[6] have estimated aeromechanics of passive rotation in flapping flight using blade-element model and compared results with experiments on artificial wings. Granlund et al[7] experimentally studied hovering motions of flat plates with a free-to-pivot hinge at the leading edge. Due to the low resistance of hinges, the plate rests against an incidence limiter during most of the translation stroke in each direction. It was also found that the plate produces a motion akin to normal-hover, but with delayed rotation. Wan et al.[8] numerically simulated a two-dimensional hinged plate with passive rotation. They found that as the stroke amplitude reduces, the averaged lift-to-drag ratio decreases. When the plate flaps with very small amplitude, the average lift can be negative. Ishihara et al[4] pointed out that due to the affection of wing elastic, the timing of the wing's rotation during the stroke reversal can be adjusted. Dai, H. et al[9] and Kang ,C.et al[10] got similar results that lift force of the wing can be strongly enhanced by about 30% by properly choosing frequency ratio. Wang,Z.J et al[11] made a comprehensive comparison between experimental, quasi-steady and computational and the results showed strong agreement. As for the relationship between the kinematical characteristics of the pitching motion and lift force generation, some researchers have tried to explain it. Passive maintenance of angle of attack during translation in crane fly wing was studied in [12].

However, the passive pitching mechanism during maneuver is still unclear. Wang, Z.J et al [13] found that fruit fly applied the passive mechanism to generate maneuver using only slight active actuation. But it is unclear what's the influence of maneuver on passive pitching mechanism, especially how the maneuver affects the lift generation.

In this study, high-fidelity three-dimensional simulations are performed to study the aerodynamics of torsional spring model in maneuver motions. The influence of maneuver on passive pitching and lift force production is discussed. An outline of the chapters shown as follow: Sec. II shows the problem formulation of hinge-linked torsional spring model and kinematics. Sec. III describes the computational method, simulation setup The simulation results and analysis on aerodynamic performance and vortex structure are presented in Sec. IV. At last, the conclusions are given in Sec. V.

II. Problem formulation

A. Flapping kinematics of wing

Figure 1 shows a three-dimensional hinge-connected rigid wing with an implemented torsional spring model. The hinge location is defined as:

$$\boldsymbol{O} = \boldsymbol{A} - (\boldsymbol{B} - \boldsymbol{A}) \cdot \boldsymbol{r} \qquad \text{Eq. (1)}$$

where $\boldsymbol{O}$, $\boldsymbol{A}$ and $\boldsymbol{B}$ are the corresponding coordinates of points $\boldsymbol{O}$, $\boldsymbol{A}$ and $\boldsymbol{B}$ shown in Eq. (1). $\boldsymbol{r}$ is the hinge ratio. The wing shape is chosen to be same as the wing shape in experiment by whitney and wood[6]. Based on information provided, the distance from the rotation axis of the wing to the leading edge is 10% of the mid-cord length.

The flapping and deviation angles are prescribed which leaves us with only one degree of freedom of the wing namely, wing pitch. Flapping and deviation of the wing is given by Eq. (2),

$$\phi(t) = \phi_m \cos(2\pi f t + \pi)$$
$$\alpha(t) = \alpha_m \sin(4\pi f t) \qquad \text{Eq. (2)}$$

where ϕ and α are the wing flapping and deviation angle, respectively. ϕ_m and α_m are the corresponding amplitudes of the two angles. f is the flapping frequency and t is the time. θ is the pitching angle, which will be obtained by the simulation, and the angle of attack equals to $90^\circ - |\theta|$.

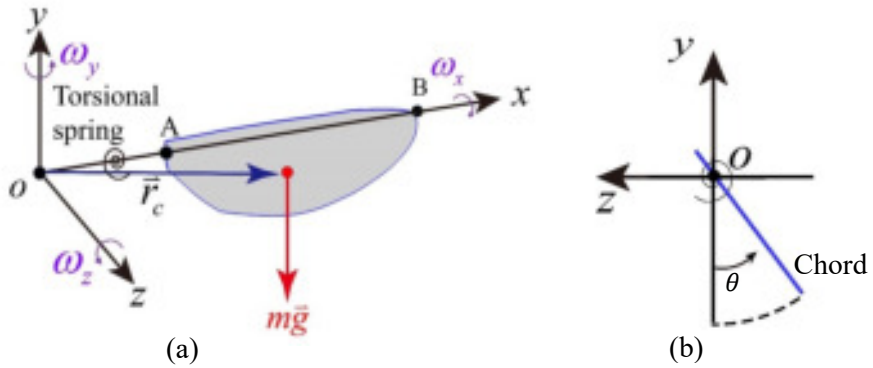

Figure 1. The wing model used in the current study. (a) illustration of the main motion direction. Wing with a hinge (at point O). Oxyz is a non-inertial frame connected with the hinge of the flapping wing. The torsional spring is aligned with the ox axis.ω_x, ω_y and ω_z are the angular velocities around the x-, y- and z-axes. c is the center of mass of the wing. $\bar{r}_c$ is the position vector of c in this local frame. m$\bar{g}$ is the gravity respectively. (b) The definition of the pitch angle.

To simulate maneuver motion, the body rotation Ω is added to perform pure yaw turn in the present study. The yaw angle rotation velocity is chosen to be constant to simplify the problem. As shown in Fig.2, the prescribed flapping motion of wing with yaw turn is illustrated. The downstroke is defined as the half stroke when the flapping direction is same as the body rotation Ω.

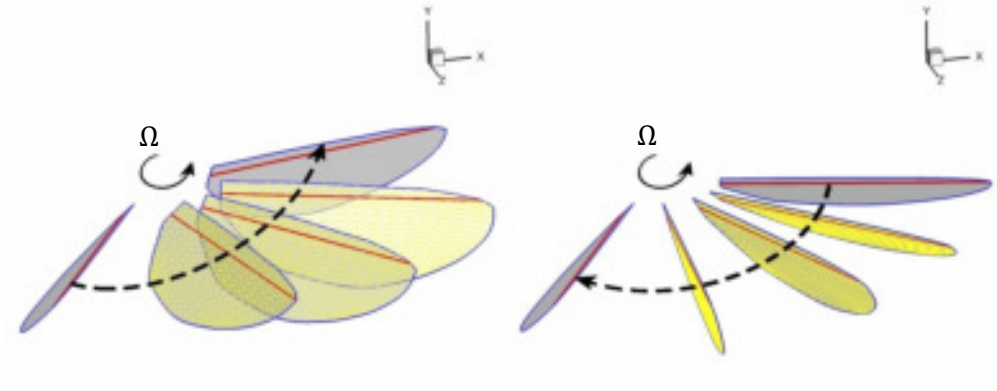

Figure 2. Schematics of wing kinematics. The downstroke is defined as the half stroke when the flapping direction is same as the yaw turn direction.

B. Governing equation of a torsional spring wing model

The dynamic equation of the pitching motion can be written as,

$$I_{xx}\dot{\omega}_x + (I_{zz} - I_{yy})\omega_y\omega_z + I_{xy}(\dot{\omega}_x - \omega_x\omega_z) + I_{yz}(\omega_y^2 - \omega_z^2) \qquad \text{Eq. (3)}$$

$$+I_{xz}\left(\dot{\omega}_z + \omega_x\omega_y\right) = M_{aero} + M_{elastic} + M_{gravity}$$

where I_{xx}, I_{yy}, I_{zz}, I_{xy}, I_{xx}, and I_{xz} are elements from the matrix of the moment of inertia of the wing. M_{aero}, $M_{elastic}$ and $M_{gravity}$ are the torques due to aerodynamic, elastic, and gravitational forces, respectively.

The aerodynamic torque M_{aero} is obtained by the surface integration of pressure p and viscous stress tensor σ, it can be expressed as,

$$M_{aero} = \int_S (\sigma \cdot \vec{n} - p\vec{n}) \times \vec{r} ds \qquad \text{Eq. (4)}$$

where $\vec{n}$ is the outer normal to the body surface, and $\vec{r}$ is the vector from mass center to certain surface element.

$$M_{elastic} = (K \cdot \theta)\vec{\imath} \qquad \text{Eq. (5)}$$

where K is the elastic modulus and $\vec{\imath}$ is the unit vector along the x-axis.

$$M_{gravity} = (\vec{\imath} \cdot (\vec{\imath}_c \times m\vec{g}))\vec{\imath} \qquad \text{Eq. (6)}$$

where m is the mass of the wing.

III. Numerical method

A. Computational method

The incompressible flow is governed by the Navier-Stokes equations, which can be written in tensor form as:

$$\frac{\partial u_i}{\partial x_i} = 0; \quad \frac{\partial u_i}{\partial t} + \frac{\partial u_i u_j}{\partial x_j} = -\frac{\partial p}{\partial x_i} + \frac{1}{Re}\frac{\partial^2 u_i}{\partial x_i \partial x_j} \qquad \text{Eq. (7)}$$

in which u_i (i=1,2,3) is the velocity components, and p is the fluid pressure. Eq.(7) is solved by using finite-difference based Cartesian grid immersed boundary method[14]. A second-order central difference scheme in space is employed. Time is advanced using a second-order accurate fractional-step method. This method was successfully applied in many simulations of flapping propulsion[15–23]. More details about this method can be found in[14,24]. Validations about this solver can be found in our previous works[25,26]. The solver has great potential for solving more complex flow conditions and higher Reynolds numbers by adding structured adaptive mesh refinement (AMR)[27,28] in the future.

B. Simulation setup

In the present study, the non-dimensional parameters of Reynolds number are defined as follow,

$$Re = \frac{U_{tip}c}{\nu} \qquad \text{Eq. (8)}$$

where U_{tip} is the non-dimensional wing tip velocity, c is the chord length, and ν denotes the kinematic viscosity. The value of yaw angle rotation velocity is chosen based on Tyson L. Hedrick and Bo Cheng's study[29]. Different natural frequencies of spring range from 50Hz to 800Hz are simulated in hovering flapping motion, the simulation results indicate that the 150 Hz to 250 Hz is a good range in hovering flapping motion which can guarantee high efficiency and large lift force. Table 1 shows a summary of all the key parameters of the present study.

Table 1. Key parameters of the present study

AR	Re	ϕ	f_n/f	Ω/ω_f
3.5	300	120°	1.5, 2, 2.5	0, 0.0625, 0.125, 0.1875, 0.25

where the ω_f demotes flapping angular velocity with $\omega_f = 2\pi f$. The lift force coefficient C_L and drag force coefficient C_D are normalized by follows,

$$C_L = \frac{F_L}{\frac{1}{2}\rho U_{tip}^2 A}, \qquad C_D = \frac{F_D}{\frac{1}{2}\rho U_{tip}^2 A} \qquad \text{Eq. (9)}$$

The computational domain has the dimension of $16c \times 16c \times 16c$ with $205 \times 177 \times 205$ grids is designed in present study. A cuboidal region around the flapping wing with high resolution grids is designed to resolve the near-field vortex structures. The zero-gradient boundary condition is applied to all lateral boundaries and a homogeneous Neumann boundary condition is used for the pressure at all boundaries.

IV. Result and Analysis

In this section, the influence of pure yaw turn on aerodynamic performance and vortex structures are presented. A parametric study on the yaw velocity is presented to explore its influence on aerodynamic performance. The vortex evolution and shedding analysis are performed by comparing the instantaneous strength of leading edge vortex, tip vortex between the prescribed pitching motion case and the passive pitching case with same yaw velocity. The mechanism of pitch bump and asymmetric force production are discussed.

A. Overall comparison of aerodynamic performance of passive pitching cases with different yaw velocities

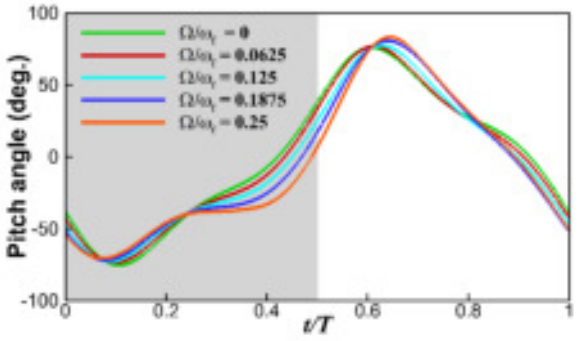

Figure 3. Comparison of pitch angle with $\phi = 120^{\circ}$ and $\Omega/\omega_f = 0, 0.0625, 0.125, 0.1875$ and 0.25, grey period is downstroke.

The comparison of the pitch angle for a full stroke is shown in Fig.3. It can be observed that with the Ω/ω_f increases, the overall pitch angle behavior becomes more asymmetric. During downstroke, the pitch bump period which is immediately after the peak, becomes more obvious. The pitch angle changes relative slow during the pitch bump period. On the contrary, with the Ω/ω_f increases, the pitch bump becomes weaker during the upstroke. The timing of the pitch peak also influenced by the yaw turn. As the Ω/ω_f increases, the timings of the pitch peak shift forward in downstroke and it shift backward in upstroke. The time period between the pitch peaks in downstroke and upstroke at the $\Omega/\omega_f = 0.25$ increases by about 20% compared to with the time period in case with $\Omega/\omega_f = 0$.

The instantaneous lift coefficient and drag coefficient are shown in Fig.4. It can be found that with the Ω/ω_f increases, the lift force and drag force production becomes asymmetric. The histories of the lift coefficient (C_L) shows that there exists a bump during down-stroke from $t = 0.3T$ to $t = 0.5T$ and it doesn't show up in up-stroke. By comparing the bump start and end time instants with pitch angle in Fig.5, it can be concluded that the aerodynamic force production bump is related to pitch angle bump during this time period. As for the drag coefficient (C_D), a similar force bump shows up but it starts at $t = 0.4T$ and ends at $t = 0.5T$.

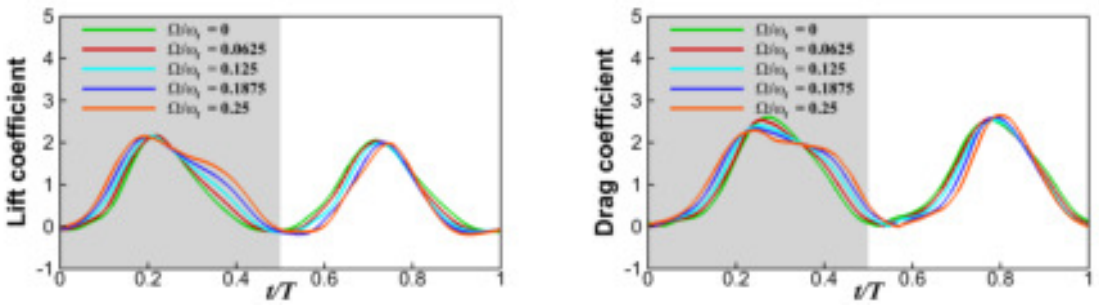

Figure 4. Instantaneous lift coefficient (C_L) and drag coefficient (C_D) with $\phi = 120^{\circ}$ and $\Omega/\omega_f = 0, 0.0625, 0.125, 0.1875$ and 0.25, grey period is downstroke.

In Table 2 and Table 3 the cycle-averaged force coefficients with different Ω/ω_f are given. The mean lift force coefficient $\bar{C}_L$ for each half stroke and mean drag force coefficient $\bar{C}_D$ for each half stroke are given, also the averaged lift-to drag ratio, which characterizes aerodynamic performance. Based on the mean lift force coefficient data in Table 2, the $\bar{C}_L$ increases with Ω/ω_f increases during down-stroke. On the other hand, the $\bar{C}_L$ decreases with Ω/ω_f increases during up-stroke. But the mean value of whole stroke shows that with Ω/ω_f increases, the $\bar{C}_L$ increses. The case with $\Omega/\omega_f = 2.5$ shows 10.4% increasing of $\bar{C}_L$ compared to the baseline case. when $\Omega/\omega_f = 2.5$, the drag force during down-stroke is about 44% higher than it during up-stroke. However, different from the lift force coefficient, the overall $\bar{C}_D$ almost keeps the same as the baseline case. Comparing to the lift-to-drag ratio in Table 3, it can be observed that the passive pitching wing performs better with yaw turn angular velocity increases.

Table 2. Cycle-averaged lift force coefficients with $\phi = 120^{\circ}$ and $\Omega/\omega_f = 0, 0.0625, 0.125, 0.1875$ and 0.25.

Ω/ω_f	$\bar{C}_L$	$\bar{C}_{L-downstroke}$	$\bar{C}_{L-upstroke}$
0	0.765（baseline）	0.731	0.798
0.0625	0.767（+0.2%）	0.815	0.719
0.1250	0.779（+1.8%）	0.909	0.648
0.2875	0.793（+3.6%）	1.018	0.567
0.2500	0.844（+10.4%）	1.148	0.541

Table 3. Cycle-averaged drag force coefficients with $\phi = 120^{\circ}$ and $\Omega/\omega_f = 0, 0.0625, 0.125, 0.1875$ and 0.25.

Ω/ω_f	$\bar{C}_D$	$\bar{C}_{D-downstroke}$	$\bar{C}_{D-upstroke}$	$\bar{C}_L/\bar{C}_D$
0	1.158（baseline）	1.141	1.178	0.661 (baseline)
0.0625	1.156（- 0.20%）	1.197	1.117	0.664 (+0.05%)
0.1250	1.160（+0.17%）	1.268	1.053	0.672 (+1.67%)
0.2875	1.167（+0.78%）	1.337	1.004	0.678 (+2.57%)
0.2500	1.185（+2.30%）	1.401	0.970	0.712(+7.72%)

B. Comparison of performance between passive pitching and prescribed pitching motion.

To better understanding the effects of passive pitching during maneuver, a prescribed pitching motion case is performed with $\Omega/\omega_f = 0.25$. The prescribed pitching motion is same as the pitching motion of passive pitching when the yaw velocity is zero. Therefore, the effects of passive pitching can be individually evaluated by comparing this prescribed pitching motion case with corresponding passive pitching case at same yaw velocity.

As shown in Fig.5, the pitch angle of passive pitching and prescribed pitching motion are presented. It can be found

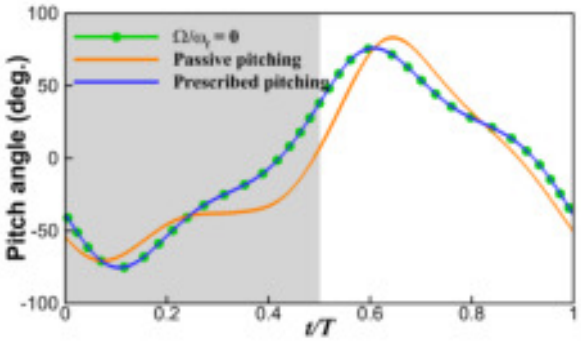

Figure 5. Comparison of pitch angle between passive pitching and prescribed pitching motion cases with $\phi = 120^{\circ}$ grey period is downstroke.

that the prescribed pitch angle is same as the pitch angle of passive pitching with $\Omega/\omega_f = 0$. The instantaneous force coefficient is presented in Fig.6, the major difference between passive pitching and prescribed pitching cases with $\Omega/\omega_f = 0.25$ are colored. As it shows, the passive pitching case generates drag force relative earlier than prescribed pitching case and lasts relative longer time period during downstroke. But the peak value of drag force of passive pitching is much smaller than the prescribed pitching motion case. It might because the pitch bump phenomenon due to passive pitching. As for the upstroke, the passive pitching case generates smaller drag force before mid-upstroke, but performs a larger drag force peak after mid-upstroke. The cycle-averaged force coefficients of these cases are shown in Table 4. When $\Omega/\omega_f = 0.25$, the lift coefficient of passive pitching case increases by 10.4% compared to passive pitching case with $\Omega/\omega_f = 0$ while the prescribed pitching motion case decreases by 4.4%. As for the drag coefficient, both of these two cases increase by 2.2%. As a result, the passive pitching case has highest lift/drag ratio during maneuver among these three cases

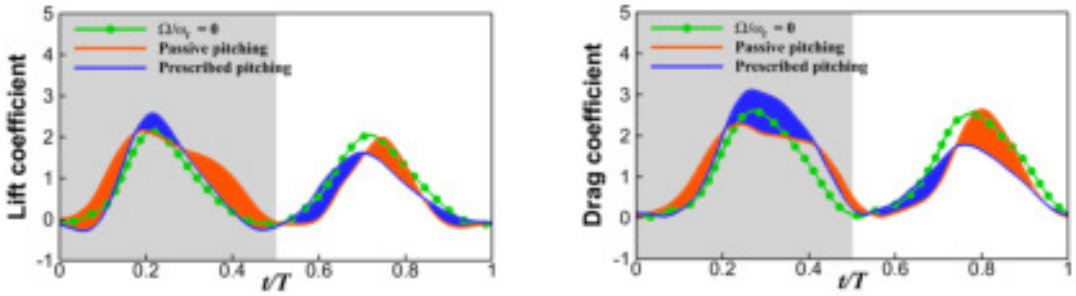

Figure 6. Comparison of instantaneous lift coefficient (C_L) and drag coefficient (C_D) between passive pitching and prescribed pitching motion cases with $\phi = 120^{\circ}$, grey period is downstroke.

Table 4. Cycle-averaged force coefficients of passive pitching and prescribed pitching motion cases

	$\bar{C}_L$	$\bar{C}_D$	$\bar{C}_L/\bar{C}_D$
Ω/ω_f= 0	0.765（baseline）	1.158（baseline）	0.660（baseline）
Prescribed pitching	0.731（-4.4%）	1.185（+2.2%）	0.617（-6.5%）
Passive pitching	0.845（+10.4%）	1.187（+2.2%）	0.712（+7.9%）

C. Comparison of vortex structure between passive pitching and prescribed pitching motion cases of $\Omega/\omega_f = 2.5$

The three-dimensional flow structures of the passive pitching and prescribed pitching motion cases with $\Omega/\omega_f = 0.25$ are visualized by plotting the iso-surface of the maximal imaginary part of complex eigenvalues of the velocity gradient tensor, Λ_{max}, which have been widely used in[24]. As shown in Fig.7, vortex formation during the down-stroke for the passive pitching and prescribed pitching motion cases are visualized with Λ_{max}=25 for the outer surface and Λ_{max}=50 for the core. To clearly present the three-dimensional flow structure at different time instant, the view is adjusted to make the wing keep a similar posture which makes comparison easier. Overall, the major flow structures in these two cases are similar but differences in vortex evolution and shedding can be observed, and these flow structures differences are highly related to the kinematics of wing. First, when $t/T = 0.2$, from (a) and (d), the LEV

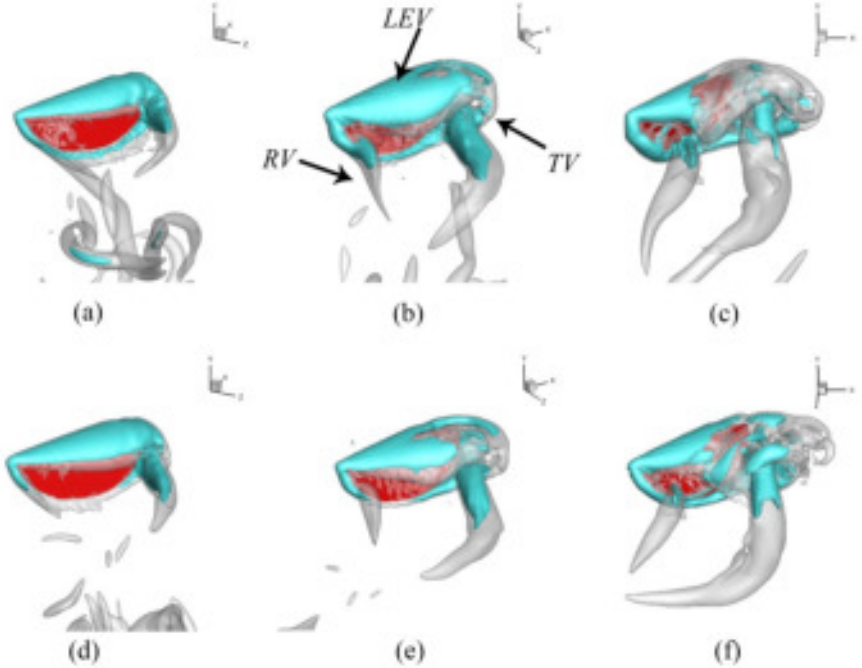

Figure 7. Comparison of vortex structures between the prescribed pitching motion case with $\Omega/\omega_f = 0.25$ at t/T= (a) 0.2, (b) 0.3, (c) 0.4. and the passive pitching case with $\Omega/\omega_f = 0.25$ at t/T= (d) 0.2, (e) 0.3, (f) 0.4.

forms along with the leading edge of the wing and it rises from the wing root to the position near wing tip, it can be found the passive pitching case has stronger LEV. The tip vortex (TV) is forms at the tip edge of the wing. When $t/T = 0.4$, for the passive pitching case, the TV becomes stronger and merges with some parts of LEV. As a result, partial LEV keeps attach on the wing surface and the rest of LEV transfers into TV. Combining with high pitch angle at this moment, it is consistent to the force production bump of this case. In comparison, in the prescribed pitching case, almost the whole LEV is going to shed which explains fast force drop during this period.

In Fig.8, slices of vorticity contours are plotted at $t = 0.2T, 0.3T$ and 0.4T. At the moement $t = 0.2T$, it can be seen from slice 1~5 that the stregth of the LEV is slight stonger in the passive pitching case, which is consistent to the relative larger C_L and C_D value at this moment. The stonger LEV in (d) may due to the higher velocity gradient which leads to a larger shear layer forming a stronger LEV. When $t = 0.3T$, plot (e) shows the strength of LEV is stronger compared to that in plot (b). Moreover, the angle of attack in (b) becomes too large that results in large drag force while the angle of attack in (e) keeps a relative smaller value, that explains the relative higher instantaneous value of drag coefficient (C_D) in Fig.6 at this moment. At the moement $t = 0.4T$, slices 1~3 in plot (f) shows that the LEV

still attach on wing surface only the LEV near wing tip detached while the LEV in (c) entirely shedded from the wing surface due to too large angle of attack.

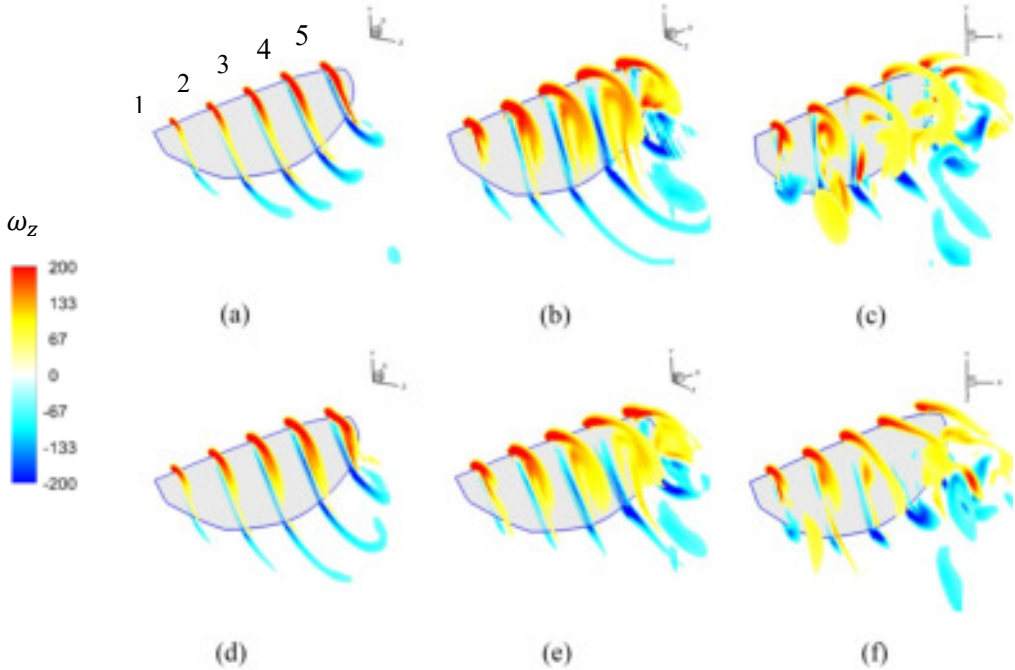

Figure 8. Comparison of slices between the prescribed pitching motion case with $\Omega/\omega_f = 0.25$ at t/T= (a) 0.2, (b) 0.3, (c) 0.4. and the passive pitching case with $\Omega/\omega_f = 0.25$ at t/T= (d) 0.2, (e) 0.3, (f) 0.4.

As for the upstroke, the three-dimensional flow structures are also visualized by the same setting as referred before. First, when $t/T = 0.65$, the passive pitching case doesn't generate LEV due to large pitch angle (small angle of attack) while prescribed motion case has a thin LEV on its wing surface. At $t/T = 0.74$, the prescribed motion case generates a stronger LEV compared to passive pitching which is consistent to the instantaneous force coefficient plot in Fig.6.when $t/T = 0.8$ which is almost the end of upstroke, (c) shows that the LEV of prescribed pitching is going to detach from the wing surface. But the LEV of passive pitching case is strong at this moment.

To further understanding the vortex evolution, slices of vorticity contours of these moments are plotted in Fig.10. As it shows in the plot (c) and (f), the prescribed pitching motion case has significant LEV on its wing surface, but the LEV near wing tip is going to detach. As a comparison, the LEV of passive pitching case at this moment is relatively smaller but with a deeper color in the core area. That means the LEV of passive pitching case is stronger and steady attaches on the wing surface. Combining with pitching angle in Fig.5 and instantaneous force coefficient in Fig.6, the only difference between these two cases at this moment is the pitch angle changing rate, which means it might because the faster pitching rotation leads to a stable LEV. Then, the passive pitching case has a relatively larger pitch angle compared to prescribed pitching case, that explains the larger drag force generation of passive pitching case during the end of the upstroke.

Combining discussion above, it can be concluded that during the downstroke, yaw velocity leads to a pitch bump in passive pitching which leads to a stronger LEV and lasts for longer time. As a result, the passive pitching case will have longer force generation period but smaller peak value. As for the upstroke, the yaw velocity results in a faster pitching changing rate which stabilizes the LEV from the mid-stroke to the end of the upstroke. As a consequence, the passive pitching case generates higher aerodynamic force peak amplitude compared to prescribed pitching motion.

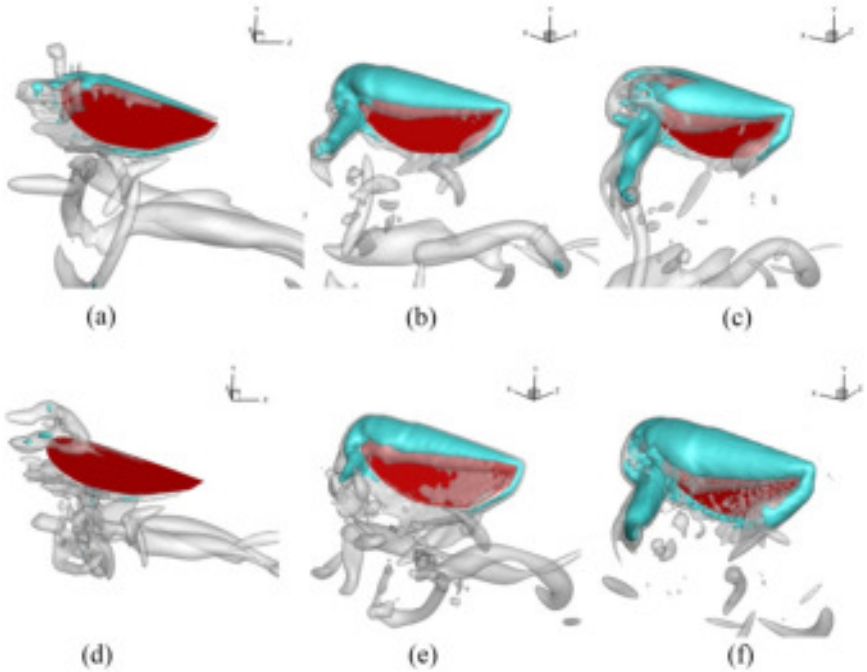

Figure 9. Comparison of vortex structures between the prescribed pitching motion case with $\Omega/\omega_f = 0.25$ at t/T= (a) 0.65, (b) 0.74, (c) 0.8. and the passive pitching case with $\Omega/\omega_f = 0.25$ at t/T= (d) 0.65, (e) 0.74, (f) 0.80.

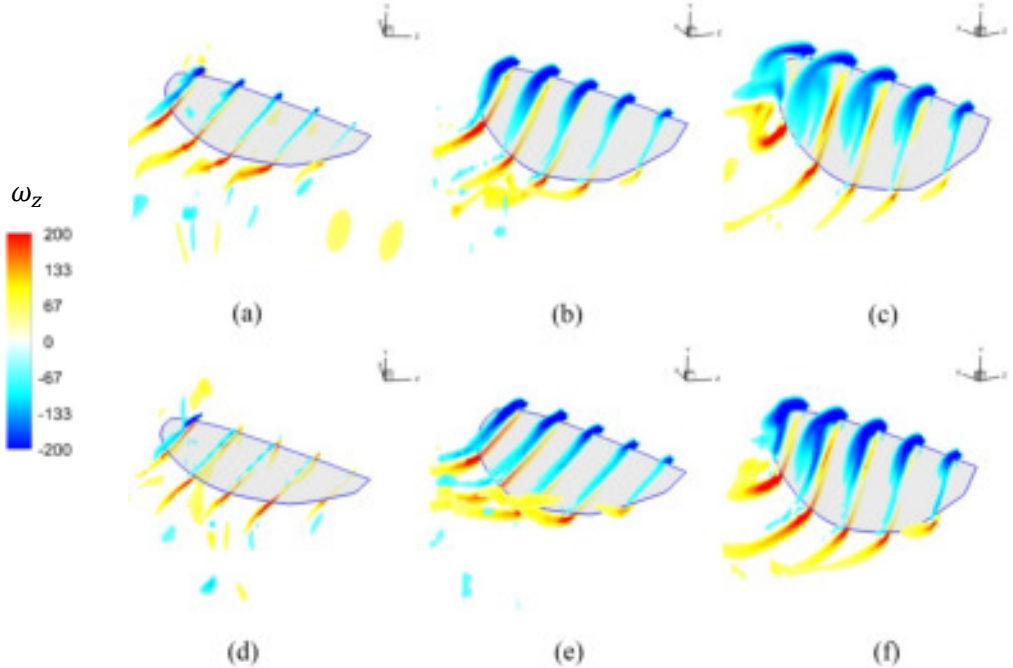

Figure 10. Comparison of slices between the prescribed pitching motion case with $\Omega/\omega_f = 0.25$ at t/T= (a) 0.65, (b) 0.74, (c) 0.80. and the passive pitching case with $\Omega/\omega_f = 0.25$ at t/T= (d) 0.65, (e) 0.74, (f) 0.80.

V. Conclusion

In this study, we present a computational study of the fluid-body interaction of a rigid wing plate three-dimensional torsional spring model performing maneuver type of flapping motion. The passive pitching flapping model is modeled as a rigid wing plate with a torsional spring on wing root. The simulation shows that the aerodynamic performance and vortex structures of the wing can be greatly influenced by the yaw angle rotation.

With Ω/ω_f increases, the drag force generation during downstroke increases and it decreases during upstroke, and similar phenenomen also appears for lift force.

By comparing the passive pitching case with prescribed pitching motion case at yaw angle rotation velocity to flapping velocity ratio is 0.25. It is found that during the downstroke, the passive pitching case generates aerodynamic force for a longer period but has smaller peak value due to pitch bump. As for the upstroke, the passive pitching case generates aerodynamics force for a shorter period but has larger peak value due to the faster pitching rotation.It is found that the mean lift force generation of passive pitching case increases by 10.4% at yaw angle rotation velocity to flapping velocity ratio is 0.25 while the prescribed pitching motion case decreases by 4.4%.

Finally, in the present study, only one wing is simulated which limits study on yaw turn on passive pitching flapping. However, it is reasonable to believe that yaw turn will have similar but opposite influence on the other wing. In that case, the overall lift force of two wings will be maintained, or slightly increased during maneuver period. Also, based on our findings that the drag force difference between downstroke and upstroke of passive pitching become smaller compared to prescribed pitching motion case, which might have a significant influence on yaw turn of the flyer. It will be attractive to link such mechanisms to the maneuver of insects in the real world to understand the flow physics behind them.

Acknowledgments

This work is supported by AFOSR FA9550-12-1-007 and NSF CEBT-1313217.

References

[1] Ennos, A., "A comparative study of the flight mechanism of Diptera," *Journal of Experimental Biology*, 1987.

[2] Ennos, A., "The importance of torsion in the design of insect wings," *Journal of experimental Biology*, 1988.

[3] Ishihara, D., Horie, T., and Niho, T., "An experimental and three-dimensional computational study on the aerodynamic contribution to the passive pitching motion of flapping wings in hovering flies," *Bioinspiration & Biomimetics*, vol. 9, 2014, p. 46009.

[4] Ishihara, D., Horie, T., and Denda, M., "A two-dimensional computational study on the fluid-structure interaction cause of wing pitch changes in dipteran flapping flight," *Journal of Experimental Biology*, vol. 212, Jan. 2009, pp. 1–10.

[5] BERGOU, A. J., XU, S., and WANG, Z. J., "Passive wing pitch reversal in insect flight," *Journal of Fluid Mechanics*, vol. 591, Nov. 2007.

[6] Whitney, J. P., and Wood, R. J., "Aeromechanics of passive rotation in flapping flight," *Journal of Fluid Mechanics*, vol. 660, 2010, pp. 197–220.

[7] Granlund, K., Ol, M., Bernal, L., and Kast, S., "Experiments on Free-to-Pivot Hover Motions of Flat Plates," 2010.

[8] Wan, H., Dong, H., and Huang, G. P., "Hovering Hinge-Connected Flapping Plate with Passive

Deflection," *AIAA Journal*, vol. 50, Sep. 2012, pp. 2020–2027.
[9] Dai, H., Luo, H., and Doyle, J. F., "Dynamic pitching of an elastic rectangular wing in hovering motion," *Journal of Fluid Mechanics*, vol. 693, 2012, pp. 473–499.
[10] Kang, C., and Shyy, W., "Scaling law and enhancement of lift generation of an insect-size hovering flexible wing," *Journal of The Royal Society*, 2013.
[11] Wang, Z. J., Birch, J. M., and Dickinson, M. H., "Unsteady forces and flows in low Reynolds number hovering flight: two-dimensional computations vs robotic wing experiments.," *The Journal of experimental biology*, vol. 207, Jan. 2004, pp. 449–60.
[12] Ishihara, D., Yamashita, Y., Horie, T., Yoshida, S., and Niho, T., "Passive maintenance of high angle of attack and its lift generation during flapping translation in crane fly wing," *Journal of Experimental Biology*, vol. 212, 2009.
[13] Bergou, A. J., Ristroph, L., Guckenheimer, J., Cohen, I., and Wang, Z. J., "Fruit flies modulate passive wing pitching to generate in-flight turns," Oct. 2009.
[14] Mittal, R., Dong, H., Bozkurttas, M., Najjar, F. M., Vargas, A., and von Loebbecke, A., "A versatile sharp interface immersed boundary method for incompressible flows with complex boundaries," *Journal of Computational Physics*, vol. 227, May 2008, pp. 4825–4852.
[15] Li, C., Dong, H., and Liang, Z., "Proper Orthogonal Decomposition Analysis of 3-D Wake Structures in a Pitching-Rolling Plate," *54th AIAA Aerospace Sciences Meeting*, Reston, Virginia: American Institute of Aeronautics and Astronautics, 2016.
[16] Liu, G., Dong, H., and Li, C., "Vortex dynamics and new lift enhancement mechanism of wing–body interaction in insect forward flight," *Journal of Fluid Mechanics*, vol. 795, 2016, pp. 634–651.
[17] Liu, G., Ren, Y., Zhu, J., Bart-Smith, H., and Dong, H., "Thrust producing mechanisms in ray-inspired underwater vehicle propulsion," *Theoretical and Applied Mechanics Letters*, vol. 5, 2015, pp. 54–57.
[18] Fish, F., Schreiber, C., Moored, K., Liu, G., Dong, H., and Bart-Smith, H., "Hydrodynamic Performance of Aquatic Flapping: Efficiency of Underwater Flight in the Manta," *Aerospace*, vol. 3, Jul. 2016, p. 20.
[19] Zeyghami, S., Bode-Oke, A. T., and Dong, H., "Quantification of wing and body kinematics in connection to torque generation during damselfly yaw turn," *Science China Physics, Mechanics & Astronomy*, vol. 60, Jan. 2017, p. 14711.
[20] Liang, Z., Dong, H., and Wei, M., "Computational Analysis of Hovering Hummingbird Flight," *48th AIAA Aerospace Sciences Meeting Including the New Horizons Forum and Aerospace Exposition*, Reston, Virigina: American Institute of Aeronautics and Astronautics, 2010.
[21] Dong, H., and Liang, Z., "Effects of Ipsilateral Wing-Wing Interactions on Aerodynamic Performance of Flapping Wings," *48th AIAA Aerospace Sciences Meeting Including the New Horizons Forum and Aerospace Exposition*, Reston, Virigina: American Institute of Aeronautics and Astronautics, 2010.
[22] Li, C., Wang, J., and Dong, H., "Proper Orthogonal Decomposition Analysis of Flapping Hovering Wings," *55th AIAA Aerospace Sciences Meeting*, Reston, Virginia: American Institute of Aeronautics and Astronautics, 2017.
[23] Dong, H., Liang, Z., and Harff, M., "Optimal Settings of Aerodynamic Performance Parameters in Hovering Flight," *International Journal of Micro Air Vehicles*, vol. 1, Nov. 2009, pp. 173–181.
[24] DONG, H., MITTAL, R., and NAJJAR, F. M., "Wake topology and hydrodynamic performance of low-aspect-ratio flapping foils," *Journal of Fluid Mechanics*, vol. 566, Nov. 2006, p. 309.
[25] Li, C., Dong, H., and Liu, G., "Effects of a dynamic trailing-edge flap on the aerodynamic performance and flow structures in hovering flight," *Journal of Fluids and Structures*, vol. 58, 2015, pp. 49–65.
[26] Wan, H., Dong, H., and Gai, K., "Computational investigation of cicada aerodynamics in forward flight," *Journal of The Royal Society Interface*, vol. 12, 2014.
[27] Chang, C.-H., Deng, X., and Theofanous, T. G., "Numerical Prediction of Interfacial Instabilities:

The Sharp Interface Method for Compressible Flows." AIAA-2011-3834, 20th AIAA Computational Fluid Dynamics Conference, Honolulu, Hawaii, June 27-30, 2011.

[28] Chang, C.-H., Deng, X., and Theofanous, T. G., "Direct numerical simulation of interfacial instabilities: A consistent, conservative, all-speed, sharp-interface method," *Journal of Computational Physics*, vol. 242, 2013, pp. 946–990.

[29] Hedrick, T. L., Cheng, B., and Deng, X., "Wingbeat Time and the Scaling of Passive Rotational Damping in Flapping Flight," *Science*, vol. 324, 2009.